# *Cis*−*Syn* Thymidine Dimer Repair by DNA Photolyase in Real Time†

Alexander W. MacFarlane, IV and Robert J. Stanley*

*201 Beury Hall, Department of Chemistry, Temple University, Philadelphia, Pennsylvania 19122*

*Received January 7, 2003; Revised Manuscript Received May 25, 2003*

ABSTRACT: DNA photolyase (PL) is a monomeric flavoprotein that repairs cyclobutylpyrimidine dimers (CPDs) via photoinduced electron transfer from a reduced flavin adenine dinucleotide cofactor ($FADH^-$) to the bound CPD. We have used subpicosecond UV transient absorption spectroscopy to measure the electron-transfer and repair kinetics of *Anacystis nidulans* DNA photolyase with dimeric and pentameric oligothymidine substrates. Here we show that the electron-transfer lifetime is 32 ± 20 ps for the pentameric substrate. Repair of the carbon−carbon double bonds (C═C) in the CPD is initiated in ∼60 ps, and bond scission appears to be completed by 1500 ps. This suggests that the repair of the two C═C bonds proceeds sequentially and that the first bond scission has a much lower activation barrier than the second. Our experiments also suggest that the semiquinone $FADH^•$ cofactor is not reduced to its catalytically active $FADH^-$ state by substrate after repair but remains in the semiquinone state. In contrast to the longer substrate, the dinucleotide substrate produced a mixture of kinetics representing bound and unbound substrate.

DNA photolyase is a monomeric flavoprotein that selectively binds and repairs CPDs[1] by the direct reversion of the cyclobutane lesion (*1*). Binding of the substrate is a light-independent process. The first step in the putative repair mechanism (*2*−*6*) requires blue light, which drives the two-electron-reduced flavin adenine dinucleotide cofactor ($FADH^-$) to an excited singlet state (**1** → **2**; see Scheme 1). This is followed by electron transfer to the CPD

$$PL_{red}^- + T<>T \xrightarrow{k_{eT}} PL_{sq}^• + T<>T^{•-}$$

with rate constant $k_{eT}$, generating the CPD radical anion $T<>T^{•-}$ and leaving the FAD cofactor in its semiquinone state, $PL_{sq}^•$ (**2** → **3**). Bond scission is thought to compete with recombination of the electron

$$PL_{sq}^• + T<>T^{•-} \xrightarrow{k_{rec}} PL_{red}^- + T<>T \ (\mathbf{3} \rightarrow \mathbf{1})$$

but this rate constant, $k_{rec}$, must be much slower than the bond scission rate since the quantum yield for repair is nearly unity (*1*). A similar argument can be made for the competition between electron transfer and internal conversion (**2** → **1**, $k_{eT} \gg k_{ic}$). The thymidine dimer radical anion subsequently undergoes reorganization spontaneously at room temperature (*7*) to form the monomer base and base anion radical

Scheme 1

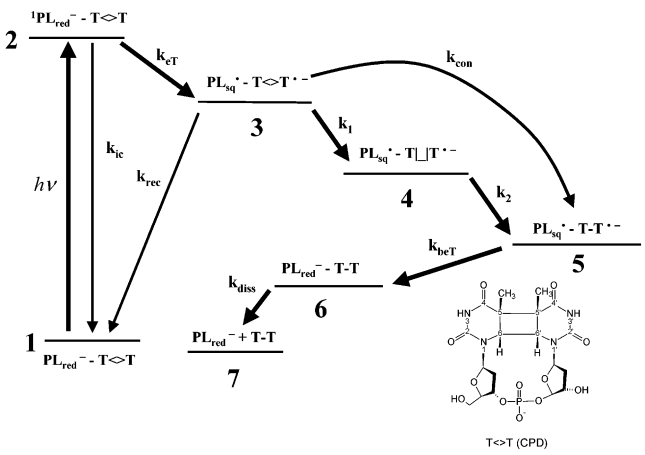


(T−$T^{•-}$, **5**). Bond breaking may involve a sequential mechanism where the C5−C5′ bond breaks with a rate constant $k_1$ followed by scission of the C6−C6′ bond ($k_2$) (or *vice versa*, in either case **3** → **4** → **5**). Another possibility is that bond scission is concerted ($k_{con}$, **3** → **5**). It is generally accepted that the electron from T−$T^{•-}$ is transferred back to $FADH^•$ to re-form $FADH^-$ ($k_{beT}$, **5** → **6**), although when this back electron-transfer step occurs has not been firmly established. Dissociation of the protein−substrate complex is thought to occur at a much later time with a rate constant $k_{diss}$ (**6** → **7**).

Because the reaction is light-driven, visible spectroscopies have been used to detect and assign intermediates in the electron-transfer and repair pathways. A significant number of transient absorption studies involving dinucleotide substrates interrogated by a visible light probe (*ca.* 400−900 nm) have been performed over the last 17 years in an effort to understand the details of the repair reaction (*6*−*17*). These time-resolved experiments suggest that repair is complete

† This research was supported by National Science Foundation Grant MCB-9982532. A.W.M. gratefully acknowledges the Petroleum Research Foundation for financial support.

* To whom correspondence should be addressed. E-mail: robert.stanley@temple.edu.

[1] Abbreviations: FAD, flavin adenine dinucleotide; $FAD_{ox}$, oxidized FAD; $FADH^•$, semiquinone FAD; $FADH^-$, fully reduced anionic FAD; CPD, cyclobutylpyrimidine dimer; T<>T, thymidine dimer; IPTG, isopropyl thiogalactoside; EDTA, ethylenediaminetetraacetic acid; DTT, dithiothreitol; PL, DNA photolyase; $PL_{ox}$, oxidized PL; $PL_{sq}^•$, one-electron-reduced PL; $PL_{red}^-$, two-electron-reduced PL.

10.1021/bi034015w CCC: $25.00 
Published on Web 06/24/2003

in ~2 ns and that the lifetime for electron transfer is ~100 ps for the T<>T dinucleotide substrate (*7*). The interpretation of the visible light probe studies is complicated precisely because the relevant radical intermediates absorb in this region. For example, some of the radicals that absorb at 410 nm are thought to be intermediates in the repair process (e.g., $FADH^{\bullet}$, $T<>T^{\bullet-}$, and $T^{\bullet-}$; see refs *3*, *4*, *7*, and *11*), while others are potentially involved in the photoreduction of $FADH^{\bullet}$ (e.g., $Trp^{\bullet+}$, $Trp^{\bullet}$, and $Tyr^{\bullet+}$; see refs *14* and *16*), a process whose physiological significance has not been established. Since these processes could be occurring in parallel, it has been difficult to assign the kinetics and develop an unequivocal model of the repair mechanism.

Instead of looking for transient intermediates in the visible region, we have focused on the ultraviolet spectral region because the repair of the CPD involves breaking the cyclobutane ring with concomitant re-formation of the C5−C6 and C5′−C6′ double bonds of the adjacent thymidines (see the CPD structure included in Scheme 1 for the numbering used in this paper). These bonds absorb strongly at 265 nm ($\epsilon$ = 9500 $M^{-1}$ $cm^{-1}$) (*18*). So, by monitoring changes at this wavelength as a function of time, we can selectively observe the thymidine bases that manifest a C=C bond in the course of repair. From these data, we can then construct a mechanism for ascertaining whether the repair of the C5−C6 and C5′−C6′ double bonds of the CPD occurs sequentially or in a concerted fashion. This paper presents our preliminary results.

Using subpicosecond resolution, we have obtained evidence that electron transfer and dimer repair occur much faster than previously reported. We also report a dramatic dependence of these kinetics on substrate length. Finally, we have observed that under our experimental conditions the flavin adenine dinucleotide cofactor is left in the semiquinone state after repair and that this state persists until reduced, either photochemically or by a chemical donor. The nature of this reactivating electron-transfer step, the electron acceptor for the repaired substrate radical anion, and the rate of dissociation of the protein−substrate complex have not yet been uncovered.

## MATERIALS AND METHODS

*Materials.* Blue Sepharose FF was purchased from Amersham Biosciences. DNA cellulose resin, lysozyme, and FMN (>98% pure) were purchased from Sigma. FAD (>98% pure) was purchased from ICN Pharmaceuticals. Desalting columns (P-6DG) were purchased from Bio-Rad. All other reagents were of the highest quality available. The reaction buffer was 50 mM Tris (pH 7.5), 10 mM 2-mercaptoethanol, 10 mM DTT, 100 mM KCl, 1 mM EDTA, and 5% glycerol, unless otherwise indicated. Storage buffer was reaction buffer with 50% glycerol. Lysis buffer was 50 mM potassium phosphate, 100 mM NaCl, 1 mM EDTA, 1 mg/mL benzamidine, and 10 mM $\beta$-mercaptoethanol (pH 8.0). Buffer A was 50 mM Tris, 1 mM EDTA, 10 mM $\beta$-mercaptoethanol, and 5% glycerol (pH 7.5) with varying amounts of KCl. Buffer B was 50 mM potassium phosphate, 1 mM EDTA, 10 mM $\beta$-mercaptoethanol, and 20% glycerol (pH 7.4) with varying amounts of KCl.

*Photolyase Protein and Substrates.* Photolyase is known to incorporate a second or antenna chromophore. This antenna pigment is folate in *Escherichia coli* and deazaflavin in *Anacystis nidulans* (*1*). *E. coli* cannot produce deazaflavin, so only FAD is present when *A. nidulans* photolyase is overexpressed in *E. coli* (*19*, *20*). The lack of this antenna molecule simplifies the electron-transfer and repair kinetics but leaves the protein fully functional (*21*, *22*).

*A. nidulans* DNA photolyase was overproduced by transforming competent JM109 *E. coli* cells (Promega) with a plasmid containing the PL gene (*20*) (pUNC1993, a generous gift of A. Sancar of the University of North Carolina, Chapel Hill, NC). The overexpression and purification of the protein have been described previously (*20*). *E. coli* cells were grown in 5 L of terrific broth at 37 °C. When the optical density of the cells at 600 nm was between 0.6 and 1.0, the cells were induced with 2 mM IPTG and grown for ~5 h. The cells were harvested by centrifugation, flash-frozen in liquid nitrogen, and stored at −80 °C. Thawed cells were lysed on ice using sonication (eight 30 s bursts at 25 W, with 30 s between bursts) and lysozyme (1 mg/mL). All subsequent steps were performed at 4 °C under yellow lights or in the dark.

A cell-free extract was obtained by high-speed centrifugation (1 h at 120000*g*). Saturated ammonium sulfate in water was added to a concentration of 45% and the mixture stirred slowly to precipitate the photolyase protein over a period of 1 h. The protein pellet was removed by centrifugation at 20000*g* for 20 min, and then a second ammonium sulfate precipitation to a concentration of 75% was performed on the supernatant. The pellet from this precipitation was suspended in a minimal quantity of buffer B with 20 mM KCl and applied to several desalting columns prepared with the same buffer. The desalted fractions were loaded onto a Blue Sepharose column (~50 mL) and washed with buffer B with 20 mM KCl until the absorption at 280 nm dropped below 1 OD unit. Elution was achieved with a 1 mL/min KCl gradient from 20 to 500 mM. The eluent was desalted with desalting columns prepared with buffer A with 20 mM KCl and loaded onto a 10 mL DNA cellulose column at 0.25 mL/min. (*23*). This step was crucial to reduce background absorption in the ultraviolet. A KCl gradient from 20 to 500 mM was used to elute the protein. The purified photolyase was concentrated and exchanged into storage buffer using 30 kDa molecular mass cutoff centrifugal concentrators (ViaSpin ultrafree) and stored at −80 °C until further use.

The purity of the protein was determined spectrophotometrically. *A. nidulans* $PL_{sq}^{\bullet}$ with no antenna cofactor present is expected to have an $A_{280}$:$A_{580}$ ratio of ~29:1. This ratio is derived from the literature value for the extinction coefficient of the semiquinone *E. coli* enzyme at 280 nm by modifying it to reflect the lack of folate (*24*) and the presence of two additional tryptophan residues found in the *A. nidulans* photolyase (*25*) as compared to the *E. coli* protein (*26*). The extinction coefficient for *E. coli* $PL_{sq}^{\bullet}$ ($\epsilon_{280}$) equals 137 300 $M^{-1}$ $cm^{-1}$, and the folate cofactor contributes 16 000 $M^{-1}$ $cm^{-1}$ to this (*24*). The folate-depleted *E. coli* protein will have an $\epsilon_{280}$ of 121 300 $M^{-1}$ $cm^{-1}$. The *A. nidulans* protein has two additional tryptophan residues, each of which will contribute 5580 $M^{-1}$ $cm^{-1}$ to the extinction coefficient. Therefore, we expect *A. nidulans* lacking the deazaflavin cofactor to have an extinction coefficient $\epsilon_{280}$ of 132 460 $M^{-1}$ $cm^{-1}$. Using the experimentally determined extinction coefficient ($\epsilon_{580}$) for the *A. nidulans* flavin semiquinone (*20*) of

4500 $M^{-1}$ $cm^{-1}$ leads to the ratio of 29:1 for purified protein. The $A_{280}$:$A_{580}$ ratio for $PL_{sq}^{\bullet}$ obtained in our laboratory after purification was ~30:1, indicating that the enzyme has been purified to homogeneity. Absorption spectra were taken using an HP 8452A photodiode array spectrometer with 2 nm resolution.

*E. coli* photolyase, reconstituted to contain only the FAD cofactor, was used for substrate-induced spectral shift experiments. This protein was overexpressed in JM109 using the pMS969 plasmid, also a gift of A. Sancar. The purification and reconstitution procedures for this photolyase have been described previously (*15*, *27*).

Dinucleotide CPDs with both 3′ and 5′ terminal phosphates were obtained by near-UV irradiation of thymidine dinucleotides (ChemGenes) in the presence of acetone. The CPDs were processed and purified as described previously (*15*) to generate the *cis*−*syn* dimer. Pentameric thymidine DNA (Transgenomic) was irradiated as described for the dinucleotide. Strands containing CPDs were purified using HPLC with a water/methanol gradient on a YMC J-Sphere $C_{18}$ column. No attempt was made to differentiate between various dimers of the $d(T<>T)_5$ oligo [e.g., d(T<>TTTT), d(TT<>TTT), etc.], but UV absorption measurements are consistent with one CPD per oligo (data not shown). The repair activity of both proteins was assayed as described previously (*15*) using 3 $\mu$M photolyase and the above substrates in reaction buffer with 50% glycerol. Both proteins repaired the substrates when irradiated with 365 nm light from a hand-held UV lamp (data not shown).

*Steady-State UV*−*Vis Spectroscopy.* Ultraviolet absorption spectra for *A. nidulans* $PL_{sq}^{\bullet}$ and $PL_{red}^{-}$ were recorded on 7 $\mu$M protein samples in reaction buffer in a 3 mm path length to determine the location of isosbestic points, especially around 265 nm. Purification of the protein as described above often resulted in a mixture of oxidation states, including $PL_{ox}$. To ensure that only a single oxidation state was present, a quartz cuvette containing the protein was purged for 20 min with argon after which the protein was photoreduced on ice using a water-filtered 60 W light bulb at a distance of ~10 cm (*8*) until no absorption of $PL_{ox}$ or $PL_{sq}^{\bullet}$ was measurable. The $PL_{red}^{-}$ sample was then left in the dark at 4 °C overnight with access to air provided by pinholes in a Parafilm cover of the cuvette to quantitatively generate the semiquinone, $PL_{sq}^{\bullet}$ (*22*). UV−vis absorption spectra were recorded on this sample after referencing the spectrometer to the reaction buffer. The protein was then photoreduced to $Pl_{red}^{-}$ as described above, and a spectrum of this state was recorded.

*Laser Spectrometer and Sample Handling.* The laser spectrometer and detection equipment have been described in detail (*15*). The titanium−sapphire laser used in these experiments generates *ca.* 100 fs duration pulses at a repetition rate of 1 kHz. The fundamental of the laser is tunable from ~770 to ~840 nm. For these experiments, a 398 nm pump beam was generated by second-harmonic generation of the fundamental in a 2 mm thick type I BBO crystal. The spectrum of the pump pulse was measured with 0.5 nm resolution. A fit of the spectrum to a Gaussian function gave a $\sigma$ of ~1.8 nm (data not shown). The corresponding Fourier transform limit of the pulse width was ~400 fs. This represents a lower limit to the pump pulse width.

Typical pump pulse energies were 4−5 $\mu$J as measured with a Si joulemeter (Molectron J3S-10). The pump beam was loosely focused into the sample cell, giving a beam diameter of ~150−200 $\mu$m and a sample volume of ~12 nL/shot. This resulted in an excitation intensity of less than ~250 $\mu J/mm^2$.

The probe beam (265 nm) was generated by mixing portions of the fundamental and second-harmonic in a 1 mm thick type II BBO crystal in a near-collinear geometry. The probe beam was separated from the fundamental and second-harmonic beams by spatial filtering followed by a UV interference filter centered about 266 nm. A Gaussian fit to the spectrum of this pulse gave a $\sigma$ width of ~1.1 nm (data not shown). This gave a Fourier transform-limited pulse width of ~450 fs. The pulse energy was ~2−3 nJ. The beam diameter at the sample was calculated to be 10 $\mu$m after focusing with a 3 in. diameter *f*/4.5 aluminized parabolic reflector (Edmund Scientific) assuming a Gaussian beam shape. The pump beam polarization was rotated to the magic angle with respect to the probe beam using a quartz half-wave plate. The angle of incidence between the pump and probe beams was ~2°.

The sample cell was designed to provide anaerobicity and sample replacement between shots. It was constructed from two 3 mm thick by 1 in. diameter sapphire windows (Meller Optics) separated by a $^3/_{32}$ in. thick silicone rubber O ring. The path length was ~1.6 mm. The cell was clamped in a circular aluminum holder by six bolts that were adjusted to make the windows as coplanar as possible. During the laser experiments, the cell was mounted in a bearing and spun at several hertz to ensure sample replacement between shots.

Excitation of the buffer alone gave rise to a Kerr lens representing the temporal cross correlation of the pump and probe pulses. The glycerol in the buffer was primarily responsible for this effect (*28*), and these buffer solutions were used to obtain the instrument response function (IRF) of the spectrometer. An IRF width of ~0.85 ps was obtained by fitting the Kerr lens transient to a function consisting of a Gaussian and an exponential function with a short lifetime

$$\mathrm{IRF} = \frac{1}{\sqrt{2\pi\sigma_{\mathrm{IRF}}}} e^{-(t-t_0)^2/2\sigma_{\mathrm{IRF}}^2} + e^{-(t-t_0)/\tau_{\mathrm{IRF}}}$$

The exponential function was necessary because the temporal profile of the Kerr lens was not symmetric ($\tau_{IRF} < 1$ ps). However, the amplitude of this exponential component was small compared to the Gaussian (a few percent), so the 0.85 ps resolution that is cited is dominated by the Gaussian component with a width of $\sigma_{IRF}$.

Experiments involving both enzyme and substrate were performed by mixing reduced protein with dried CPD-containing DNA in a $N_2$-purged glovebag just prior to loading the sample cell. The ratio of substrate to protein was not less than 3:1, so extensive signal averaging could be performed. Typically, 20−30 $\mu$M protein solutions were used so that the overall UV absorption at 265 nm was less than 0.8 before the addition of substrate. The pentameric substrate has an intrinsic extinction coefficient of ~29000 $M^{-1}$ $cm^{-1}$ at 265 nm, limiting the substrate:protein molar ratio for these experiments to ~5:1.

Experiments were continued until ~50% of the substrate was repaired. This allowed for ~1 h of signal averaging at

Table 1.

| species | $\tau_1$ (ps) | $\tau_2$ (ps) | $\tau_3$ (ps) | $A_2/A_1$[a] | $A_3/A_1$ | $A_3/A_2$ |
|---|---|---|---|---|---|---|
| $FADH^-$ | 4 | 121 | − | 9.6 | − | − |
| $FMNH^-$ | 41 | 843 | − | 6.3 | − | − |
| $PL_{sq}^{\bullet *}$ | 16 | 3300 | 13700 | 0.7 | −0.5 | −0.75 |
| $PL_{red}^-$ | 7 ± 3 | 850 ± 70 | − | 3.2 ± 1.5 | − | − |
| $d(T<>T)_2-PL_{red}^-$ (5:1) | 9 ± 3 | 500 ± 240 | 10200 ± 5000 | 1.9 ± 0.8 | −0.1 ± 0.1 | −0.1 ± 0.1 |
| $d(T<>T)_2-PL_{red}^-$ (10:1) | 6.5 ± 0.8 | 415 ± 270 | 6167 ± 4010 | 1.8 ± 0.7 | −0.2 ± 2 | 0.1 ± 0.9 |
| $d(T<>T)_2-PL_{red}^-$ (20:1) | 38 ± 10 | 589 ± 70 | 8500 ± 2900 | 1.4 ± 0.1 | −1.3 ± 0.3 | −0.9 ± 0.2 |
| $d(T<>T)_5-PL_{red}^-$ (4:1) | 32 ± 20 | 600 ± 300 | 6500 ± 5100 | 1.7 ± 0.8 | −1.5 ± 0.7 | −1.0 ± 0.3 |

[a] $A_1$ and $A_2$ are negative.

1 kHz. At the end of this period, the sample integrity and anaerobicity were verified by UV−vis spectroscopy. Under these conditions, some sample degradation was noted; however, it appeared that the protein was stable against oxidation to the semiquinone even at the highest pump power (this was substrate-dependent; see below). All kinetic data were obtained at room temperature in the dark, while sample loading was performed under yellow light.

*Data Analysis.* All calculations were performed on ≥1 GHz AMD Athlon-based PCs. The transient data were analyzed using two different methods. This was done to make sure the Kerr lens did not affect the fitted parameters. A "convolute and compare" algorithm was used to fit the raw data as described below. In the second method, the Kerr lens was fitted with a Gaussian function and the function subtracted from the raw data. The result was fitted using a sum of exponentials as described below. Both methods produced parameters that were the same within error. Error estimates accompanying measurements represent the standard deviation of fitted parameters for at least three scans except for the 10:1 $d(T<>T)_2$:$PL_{red}^-$ experiment, which was performed twice. The parameters from single scans are indicated when no standard deviation is given.

A convolute and compare algorithm with up to three exponential functions and the IRF was used to fit the raw data (the fast exponential component used to fit the IRF, typically less than 1 ps, is omitted from the data presented in Table 1). This method has been used widely (*29*−*31*). Briefly, a set of *n* exponential functions with lifetimes of $\tau_1-\tau_n$ are convoluted with the fitted IRF. Amplitudes for this set of functions, $A_1-A_n$, respectively, are obtained by a linear least-squares fit of the convoluted exponential functions with the experimental data. A test function is constructed

$$\text{test}(\tau_i,A_{\text{IRF}},t_0;t) = A_{\text{IRF}}(\text{IRF}) + \sum_{i=1}^{n} A_i e^{-(t-t_0)/\tau_i} \otimes \text{IRF}$$

where ⊗ indicates the convolution process, $t_0$ is the excitation zero of time, and $A_{\text{IRF}}$ is the amplitude of the IRF used to fit the Kerr lens signal. The sum of the residuals of the fit [residuals = $\sqrt{(\text{test} - \text{data})^2}$] is minimized using either a simplex or Marquardt−Levenberg technique (MATLAB 6.5, The Mathworks) until no further improvement was obtained. The tabulated parameters presented herein are those obtained from the convolute and compare algorithm.

A check on this analysis was performed by subtracting the Kerr lens artifact from the data and fitting this decay using a multiexponential function. This was done by first fitting the Kerr lens transient to a Gaussian function for a given data set such that $t < 0.3$ ps. The Gaussian obtained from this procedure was then subtracted from the data set. This treated data were fitted to a sum of either two or three exponentials beginning after the minimum in the signal, typically around a *t* of >1.2 ps. By this time, the contribution of the instrument response to the kinetics has become negligible. OriginLab 7.0 (Microcal) was used to fit the multiple-exponential functions. No significant difference in the amplitudes, time constants, or number of components between the above approach and the convolute and compare algorithm was evident within the standard deviation obtained using the convolute and compare algorithm.

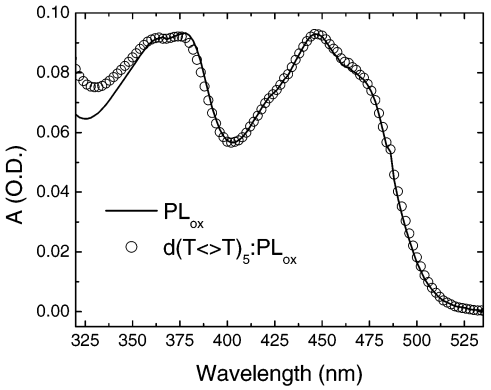


FIGURE 1: UV−vis absorption spectra of folate-depleted *E. coli* $PL_{ox}$ (−) and the $d(T<>T)_5-PL_{ox}$ complex (○) in a 5:1 molar ratio. The $PL_{ox}$ concentration was 8 μM for both spectra. A spectral blue shift of ∼4 nm can be seen for the $S_0 \rightarrow S_2$ transition (centered around 370 nm) for the substrate−protein complex.

## RESULTS

*Spectral Shift Due to Substrate Binding.* To perform the time-resolved experiments, it was necessary to identify the minimal length substrate that bound tightly to PL while avoiding an overly high background absorption at 265 nm. A spectroscopic assay was used to determine whether a short thymidine oligomer containing a CPD gave productive binding compared to a longer substrate (*15*, *27*). To this end, a $d(T<>T)_5$ substrate was combined with oxidized folate-depleted *E. coli* photolyase. A blue spectral shift (4 ± 2 nm) was observed for the $S_0 \rightarrow S_2$ band (∼370 nm) by steady-state UV−vis spectroscopy (Figure 1). This shift is the same, within experimental error, as that obtained in our laboratory for a $d(T<>T)_{18}$ substrate (*15*) and by Jorns *et al*. (*27*), although a concomitant blue shift of the $S_0 \rightarrow S_1$ band (∼1.7 nm) was not observed. This smaller shift was resolved in the previous experiments by using a higher-resolution spectrometer (0.5 nm); therefore, the 1.7 nm blue shift was not expected to be resolved using the 2 nm band-pass

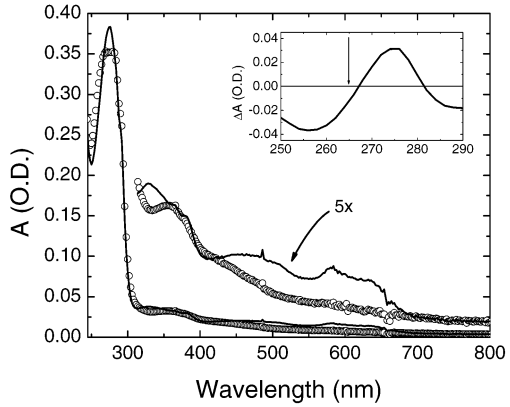


FIGURE 2: UV absorption spectra of $PL_{sq}^{\bullet}$ (—) and $PL_{red}^{-}$ (○) under anaerobic conditions. The concentration was 7 $\mu$M and the path length 0.3 cm. The region from 312 to 800 nm is magnified by a factor of 5. The inset is the difference spectrum ($PL_{sq}^{\bullet} - PL_{red}^{-}$) from 250 to 290 nm, where the arrow indicates the probe wavelength used in the transient absorption experiments.

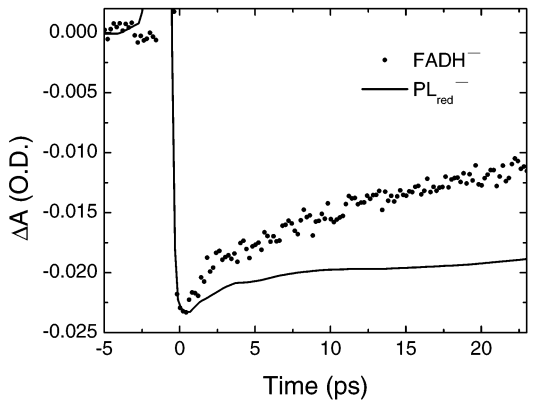


FIGURE 3: Two color pump−probe time-resolved decay of 125 $\mu$M $FADH^-$ in pH 8.2 buffer and 30% glycerol (···) compared to that in 30 $\mu$M $PL_{red}^{-}$ in reaction buffer (—). The pump wavelength was 398 nm, and the probe wavelength was 265 nm. The protein decay has been scaled to the free flavin decay for comparison. Free $^1FADH^-$ decays more quickly because of base stacking interactions between the isoalloxazine and adenine rings. The level of this quenching is significantly reduced in photolyase. The negative $\Delta A$ is assigned as a ground-state bleach.

spectrometer. No shift was observed for dinucleotide CPDs containing either two or three backbone phosphates at a substrate:protein molar ratio of up to 20:1 (*15*). These results suggest that the binding geometry for $d(T<>T)_5$ is similar to that of a longer oligo, while the $d(T<>T)_2$ substrate−protein complex has a different geometry (*32*).

*Ultraviolet Absorption Spectra of FMNH⁻ and Photolyase.* The extinction coefficient of $PL_{red}^{-}$ is ∼3000 $M^{-1}$ $cm^{-1}$ at the excitation wavelength of ca. 400 nm (*20*). However, it is the extinction coefficient at 265 nm that will determine the initial magnitude of the transient absorption signal, in the absence of any excited-state absorption. We estimate that the molar extinction coefficient at 265 nm ($\epsilon_{265}$) for the fully reduced anionic isoalloxazine moiety equals ∼16000 $M^{-1}$ $cm^{-1}$. This value is based on the extinction coefficient of $FMNH^-$ at this wavelength obtained in our laboratory by steady-state UV−vis absorption spectroscopy on FMN samples photoreduced in pH 8.2 buffer using oxalate as a reductant (*33*) (data not shown). We show below that excitation at ca. 400 nm leads to a net ground-state bleach of the flavin chromophore probed at 265 nm.

Since the transient absorption experiments utilized a 265 nm probe, it was necessary to obtain the steady-state UV spectra of *A. nidulans* $PL_{sq}^{\bullet}$ and $PL_{red}^{-}$. After photoexcitation of the $FADH^-$ cofactor in $PL_{red}^{-}$, electron transfer to the CPD will leave the flavin in its semiquinone state, $FADH^{\bullet}$ (*11*). With the probe wavelength set slightly off of the isosbestic point at 267 nm, the kinetics of this electron-transfer reaction will be evident. However, to differentiate between the electron-transfer and repair steps, it is necessary to account for the difference in the extinction coefficients between $PL_{red}^{-}$ ($FADH^-$) and $PL_{sq}^{\bullet}$ ($FADH^{\bullet}$) at 265 nm and compare this difference to the extinction coefficient resulting from the complete repair of the CPD.

Spectra for a 7 $\mu$M sample of photolyase are shown in Figure 2. The UV difference spectrum [$\Delta A(PL_{sq}^{\bullet} - PL_{red}^{-})$] exhibited isosbestic points at 267 ± 2 and 281 ± 2 nm (see the inset in Figure 2). The value of the UV difference spectrum at 265 nm gives an absorbance change $\Delta A$ of −0.012 ± 0.001. This corresponds to a change in $\Delta\epsilon_{265}$ of −5800 $M^{-1}$ $cm^{-1}$. Full repair of the CPD will result in an extinction coefficient of approximately 19 000 $M^{-1}$ $cm^{-1}$, corresponding to the appearance of the two C=C bonds. Thus, changes in the transient absorption decay at 265 nm will primarily reflect the absorption of the repaired CPD. This assumes that any excited-state absorption due to $^1FADH^-$ is negligible and that the CPD radical anion extinction is small compared to 19 000 $M^{-1}$ $cm^{-1}$. We discuss these two points below.

*Control Experiments: Kinetics of $^1FADH^-$, $^1FMNH^-$, and $^1PL_{red}^{-}$ Probed at 265 nm.* As a control, the decay of $^1FADH^-$ in pH 8.2 phosphate buffer was monitored at a $\lambda_{probe}$ of 265 nm for a 125 $\mu$M solution (Figure 3). $FADH^-$ was generated from $FAD_{ox}$ under anoxic conditions by photoreduction in the presence of oxalate (*33*). The change in absorbance for $^1FADH^-$ measured 2 ps after excitation was linear with pump power up to at least 5.2 $\mu$J/pulse (correlation coefficient $r = 0.998$, data not shown), indicating that the observed kinetics are the result of a one-photon absorption. The $^1FADH^-$ decay could not be fitted to a single exponential, in agreement with results from Enescu *et al.* (*34*) using visible probe pulses. A two-component fit gave a $\tau_1$ of ∼4 ps and a longer-lived component that depended on the length of the acquisition window (Table 1). The 4 ps lifetime is shorter than that obtained by Enescu *et al.* ($\tau_1$ = 17 ps), who used 312 nm subpicosecond excitation pulses (*34*). However, we have shown that there is a fast component ($\tau_1 \sim 4$ ps) in the decay of $^1FAD_{ox}$ that is due to internal conversion caused by base stacking of the adenine with the isoalloxazine ring (*35*). The results for $^1FADH^-$ are consistent with those measurements.

The kinetics of $^1FMNH^-$ were obtained under the same conditions as those for $^1FADH^-$ to ascertain whether the adenine moiety of FAD, which absorbs at 265 nm, affected the observed kinetics (data not shown). Again, the kinetics require two lifetimes for an adequate fit. The loss of base stacking gives the expected result that $^1FMNH^-$ has a significantly slower first component than $^1FADH^-$, ∼41 ps (compared to ∼60 ps from Enescu and co-workers). The lifetimes and amplitude ratios are given in Table 1.

The amplitude of the bleach ($\Delta A$) equals approximately −23 mOD. This amplitude is less than expected if the signal

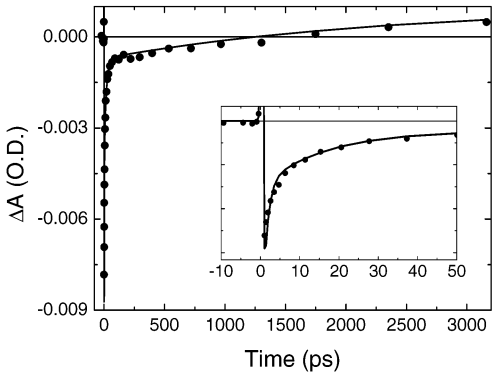


FIGURE 4: Pump−probe time-resolved decay of $PL_{sq}^{\bullet}$. The pump wavelength was 398 nm, and the probe wavelength was 265 nm. The large transient bleach and subsequent $^2PL_{sq}^{\bullet} \rightarrow PL_{red}^{-}$ reduction ($\tau \sim 16$ ps) are more easily seen in the inset. The solid line is the fit of a three-exponential function to the data (see Table 1).

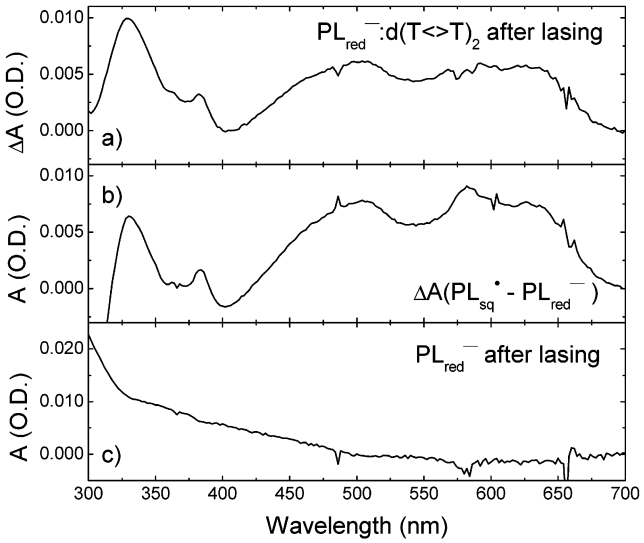


FIGURE 5: (a) Steady-state absorption spectrum of the $d(T<>T)_2-PL_{red}^{-}$ complex with a molar ratio of 20:1 after ~1 h of lasing with 4 $\mu$J, 400 fs pulses at 398 nm. The protein concentration was 30 $\mu$M. The reference for this spectrum was the reduced substrate−protein complex before irradiation. (b) Steady-state difference absorption spectrum of $PL_{sq}^{\bullet} - PL_{red}^{-}$ in the absence of substrate (from Figure 2). (c) Like panel a but without substrate. The increasing baseline to the blue is due to scatter.

were due solely to a ground-state bleach. We estimate that 30% of the sample volume is excited by the 5 $\mu$J pulse, based on photoselection and optical pumping considerations. This leads to an excited-state absorption extinction coefficient ($\epsilon_{ESA}$) of approximately 12 000 $M^{-1}$ $cm^{-1}$. Taken together, we assign the 265 nm transient in both $FADH^-$ and $FMNH^-$ samples to a net ground-state bleach of the isoalloxazine moiety.

The excited-state decay of $PL_{red}^{-}$ (30 $\mu$M) was measured to compare it with the kinetics of both the cofactor in buffer and the substrate−protein complexes. The signal for photolyase without substrate ($^1PL_{red}^{-}$) becomes negative due to the ground-state bleach of the $FADH^-$ cofactor, then increases slowly, and approaches a $\Delta A$ of 0 after ~3000 ps (only the first 25 ps of the data are shown in Figure 3 to facilitate comparison with $^1FADH^-$; the full scan range is shown in Figure 6). Two lifetimes were necessary to fit this decay, with most of the amplitude in the longer $\tau_2 \sim 850$ ps component, and a small amplitude component ($\tau_1$) with a

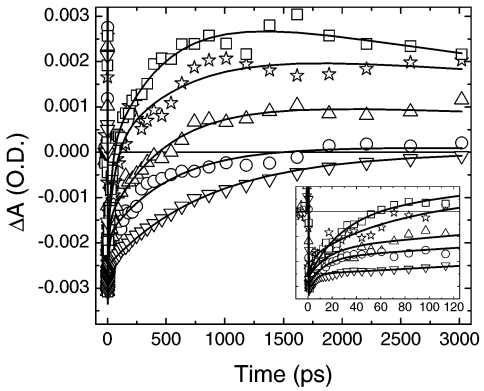


FIGURE 6: Transient decay of $d(T<>T)_n-PL_{red}^{-}$ complexes for an $n$ of 2 or 5 over 3000 ps. The $d(T<>T)_2$:$PL_{red}^{-}$ molar ratio was varied among 5:1 (○), 10:1 (△), and 20:1 (☆), and the $d(T<>T)_5$:$PL_{red}^{-}$ molar ratio was 4:1 (□). The $PL_{red}^{-}$ decay (▽) is included for reference. The decays have been baseline-normalized and then normalized to the $d(T<>T)_5-PL_{red}^{-}$ decay for comparison. A positive $\Delta A$ indicates repair of $d(T<>T)_n$. The inset shows the zero crossing for the $d(T<>T)_2-PL_{red}^{-}$ (20:1) and $d(T<>T)_5-PL_{red}^{-}$ (4:1) complexes in detail. The solid lines are fits to the decays as described in the text.

lifetime of ~7 ps (see Table 1). Both amplitude components are negative, and $A_2/A_1 = 3.2 \pm 1.5$. The lack of any new kinetic component in the fit compared to the simple flavins suggests that no electron transfer takes place in the absence of substrate. Extensive photolysis of the protein produced some degradation of the sample, but no oxidation to the semiquinone was seen, in contrast to the observations of Langenbacher *et al.* for the *E. coli* protein (*7*).

*Kinetics of the Photoreduction of $PL_{sq}^{\bullet}$ Probed at 265 nm.* An earlier report of the ultrafast photoreduction of $PL_{sq}^{\bullet}$ (*14*, *16*) prompted us to examine this phenomenon under our experimental conditions. The photoreduction process begins following excitation of the flavosemiquinone by electron abstraction from a nearby Trp residue:

$$^2PL_{sq}^{\bullet}\cdots TrpH \xrightarrow{h\nu} PL_{red}^{-}\cdots TrpH^{\bullet+}$$

The Trp radical cation then abstracts an electron from another Trp (or Tyr in the case of *A. nidulans*), ultimately ending in the release of a proton to solution for stabilization of the reduction of the protein to $PL_{red}^{-}$.

The transient decay of $^2PL_{sq}^{\bullet}$ with a $\lambda_{probe}$ of 265 nm following 398 nm excitation is shown in Figure 4. This transient was fitted to three exponential functions with the following lifetimes: $\tau_1 \sim 16$ ps, $\tau_2 \sim 3$ ns, and $\tau_3 \sim 14$ ns (see Table 1). The first two components have negative amplitudes, while the long time component has a positive amplitude where $A_2/A_1 = 0.7$ and $A_3/A_1 = -0.5$. The 16 ps component (better seen in the inset of Figure 4) is a factor of 2 shorter than the 30 ps lifetime observed by Aubert *et al.* (*14*) for the $^2PL_{sq}^{\bullet} \rightarrow PL_{red}^{-}$ photoreduction in *E. coli* photolyase. The lifetimes of the longer components are consistent with the 10 ns phase observed in *E. coli* and probably are an indication of the subsequent electron abstraction events. In our work, the 265 nm transient signal increased somewhat monotonically and passed through a $\Delta A$ of 0 at ~1500 ps. This is consistent with the slightly greater absorption of $PL_{red}^{-}$ at 265 nm, compared to that of $PL_{sq}^{\bullet}$ (see Figure 2). It is possible that absorption changes at this

wavelength are due to the Trp → $Trp^{\bullet+}$ conversion; however, we think the contribution is small. The transient absorption spectrum of the Trp → $Trp^{\bullet+}$ conversion appears to have an isosbestic point around 265 nm (*36*). More precise measurements are needed to resolve this discrepancy. However, the semiquantitative agreement between the two lifetimes highlights the importance of using short pulses to obtain the kinetics of the protein−substrate complexes.

*Semiquinone Buildup in Short Pulse-Irradiated Substrate−Photolyase Complexes.* Initial transient absorption experiments on substrate−photolyase complexes were performed using 398 nm pump and 265 nm probe pulses with subpicosecond resolution. The substrate was mixed with $PL_{red}^-$ at a minimum molar ratio of 3:1 under anaerobic conditions, and a UV−vis spectrum was taken to verify the oxidation state of the protein. The sample was then irradiated in the laser spectrometer to obtain kinetic data. However, in the course of these experiments, we were surprised to find that substrate consumption during a run would slow significantly after approximately one turnover of the substrate by the protein. This effect did not depend on the rate of sample spinning.

After the transient absorption measurement (∼1 h), another UV−vis spectrum was taken to determine the extent of substrate repair and to verify that the sample cell had maintained anaerobicity. Surprisingly, significant amounts of $PL_{sq}^{\bullet}$ were observed consistently after laser excitation of the substrate−protein complex (Figure 5a), the spectrum of which matched the UV−vis difference spectrum obtained at the steady state without any laser excitation and in the absence of substrate (Figure 5b, from the data used in Figure 2). However, when the protein alone was irradiated with 398 nm excitation pulses, no change in the absorption spectrum was detected (Figure 5c). As a second control, the sample cell was spun extensively without lasing and left overnight in the dark at 4 °C on several occasions. No semiquinone buildup was evident under these conditions. These results suggest that $PL_{sq}^{\bullet}$ formed after repair may persist under conditions where the excitation pulse is short compared to the lifetime to initiate the $PL_{sq}^{\bullet}$ → $PL_{red}^-$ photoreduction (∼16 ps). We discuss the implications of this below.

*Electron-Transfer and Repair Kinetics Measured at 265 nm.* Excited-state kinetics were measured for $d(T<>T)_2-PL_{red}^-$ and $d(T<>T)_5-PL_{red}^-$ complexes with 850 fs resolution following excitation at 398 nm. Again, the probe wavelength was 265 nm. To avoid the spectral complications due to semiquinone buildup, transient absorption measurements were taken in which the excitation volume was overlapped by a loosely focused 632.8 nm, 5 mW continuous wave (cw) helium−neon (HeNe) laser beam. The cw HeNe beam ensures that any semiquinone formed in the excitation volume will be photoreduced. However, it is unlikely that the cw HeNe beam altered the measured kinetics since the odds of absorbing a photon from such a weak source in the 3 ns experimental time window are vanishingly small. All of the transient absorption data for the substrate−protein complexes presented below were recorded under these conditions, and no semiquinone buildup was observed in the sample once this procedure was instituted.

Transient absorption decays for the $d(T<>T)_n-PL_{red}^-$ complexes ($n = 2$ or 5) are shown in Figure 6. The result for $PL_{red}^-$ is given for reference. The lifetimes for the exponential model fits (solid lines) are given in Table 1. Since the decays do not come to baseline in the 3 ns measurement window, the amplitudes and lifetimes for the longest component are only semiquantitative. However, the $A_2/A_1$, $A_3/A_1$, and $A_3/A_2$ amplitude ratios should be comparable between complexes and are given in Table 1.

The decay of the $d(T<>T)_2-PL_{red}^-$ complex was obtained as a function of molar ratio. The substrate:protein molar ratio was varied between 5:1 and 20:1. Three components were necessary to obtain a reasonable fit to the data. The decay of the $d(T<>T)_2-PL_{red}^-$ complex with a molar ratio of 5:1 gave a very fast component ($\tau_1 \sim 9 \pm 3$ ps) that is, within experimental error, the same as the 7 ps component for $PL_{red}^-$. However, unlike the protein alone, the transient signal crosses a $\Delta A$ of 0 at approximately 1600 ps, indicating that repair of the dinucleotide substrate is taking place.

Increasing the concentration of the $d(T<>T)_2$ substrate reduced the time at which the zero crossing occurred and increased the final absorption at long times, both of which are consistent with ultrafast electron transfer followed by repair. It is difficult to assign an electron-transfer lifetime for this substrate since we could not achieve a sufficiently high substrate concentration to see an asymptote in the fast component ($\tau_1$) for the $d(T<>T)_2$ substrate, but it is likely somewhat smaller than the $\tau_1 = 38 \pm 10$ ps lifetime obtained for the 20:1 sample. The zero crossings are ∼1600, 400, and 100 ps for the 5:1, 10:1, and 20:1 molar ratios, respectively, which is indicative of a greater degree of repair. The trend in the ratio of amplitudes upon going from low to high molar ratios of dinucleotide substrate illustrates this point: $A_2/A_1$ trends from 1.9 to 1.4, while $A_3/A_1$ trends from −0.1 to −1.3. This latter trend shows that the degree of repair is small in the 5:1 dinucleotide case compared to the 20:1 case. The shift in the zero crossing as a function of substrate suggests that the $d(T<>T)_2-PL_{red}^-$ transients represent a sum of decays from substrate−protein complexes and free protein.

Both $\tau_1$ and the zero crossing time appear to be fastest for the $d(T<>T)_5-PL_{red}^-$ complex with an average molar ratio of 4:1. The transient in Figure 6 is an average of data for molar ratios between 3:1 and 5:1. This range was limited by the overall UV absorption of the pentameric substrate. No trend in the lifetimes with the substrate:protein molar ratio was evident over this range within the signal to noise ratio range. However, the amplitude ratios reflect the fact that the pentameric substrate is more productively bound than the dinucleotide substrate. The $A_3/A_1$ ratio of approximately −1.5 shows that more repair is evident for the pentameric substrate than for the dinucleotide substrate.

If we assume the kinetics of the pentameric substrate−protein complex represent the true kinetics regardless of substrate length, then it should be possible to fit the dinucleotide decays to a weighted sum of the pentameric decay and the decay of $PL_{red}^-$ without any substrate. This is shown in Figure 7 where the solid lines represent the function $F(t)$, where $F(t) = c_5[d(T<>T)_5-PL_{red}^-](t) + c_{PL}[PL_{red}^-](t)$. The coefficients $c_5$ and $c_{PL}$ are the weighting coefficients of the $[d(T<>T)_5-PL_{red}^-](t)$ and $[PL_{red}^-](t)$ decays, respectively. These coefficients are given in Table 2 and were obtained by simultaneously fitting all of the data over a time window from 2 to 3000 ps. The coefficients for each substrate concentration in Table 2 have been normalized to unity for comparison. The agreement between the fits and

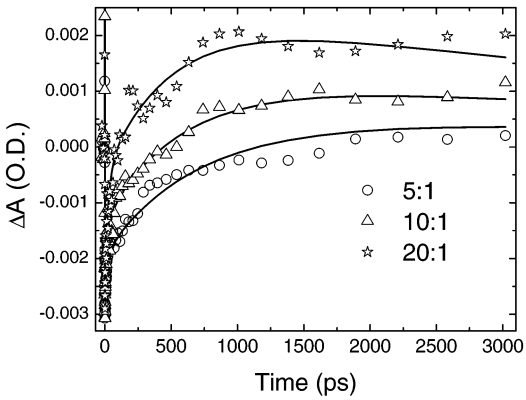


FIGURE 7: Fit (—) of the sum of the $d(T<>T)_5-PL_{red}^-$ and $PL_{red}^-$ decays to the dinucleotide decays, at $d(T<>T)_2$:$PL_{red}^-$ molar ratios of 5:1 (○), 10:1 (△), and 20:1 (☆). The coefficients for the fit are given in Table 2.

Table 2

| species | $c_5$ | $c_{PL}$ |
|---|---|---|
| $d(T<>T)_2-PL_{red}^-$ (5:1) | 0.20 | 0.80 |
| $d(T<>T)_2-PL_{red}^-$ (10:1) | 0.45 | 0.55 |
| $d(T<>T)_2-PL_{red}^-$ (20:1) | 0.83 | 0.17 |

the data is reasonable, lending support for this model. From the coefficients, it appears that only ∼20% of the dinucleotide substrate is effectively bound for repair at the 5:1 substrate:protein molar ratio. Thus, the largest contribution to the signal at this molar ratio is the protein decay. Even at 20:1, there is still a significant contribution (17%) from the free protein.

Using these coefficients, it should be possible in principle to extract an effective association constant

$$K_A^{\text{eff}} \frac{c_5[PL_{red}^-]}{(c_{PL}[PL_{red}^-])([d(T<>T)_2] - c_5[PL_{red}^-])}$$

where the indicated concentrations are the initial values. $K_A^{\text{eff}}$ can then be compared to a $K_A$ of 18 000 $M^{-1}$ as determined from gel shift assays (*23*). The $K_A^{\text{eff}}$ obtained from this analysis is not constant using the coefficients from Table 2. However, our results suggest that the association constant for the dinucleotide substrate derived from gel shift assays is an overestimate.

A fit of the $d(T<>T)_5-PL_{red}^-$ decay required three components (see Table 1) which match those obtained for the 20:1 $d(T<>T)_2-PL_{red}^-$ sample within experimental error. The fastest time constant $\tau_1$ equals 32 ± 20 ps. To assign this lifetime as the electron-transfer lifetime, it is necessary to account for the extinction of the CPD radical anion, $T<>T^{\bullet-}$. To our knowledge, the extinction coefficient of this species has not been measured in the UV. However, Hayon has shown that the extinction coefficient of dihydrothymine radical anion is less than 1600 $M^{-1}$ $cm^{-1}$ at 265 nm and pH 5 (*37*). If we assume that this valve is not very sensitive to pH, then the sum of the $T<>T^{\bullet-}$ extinction coefficient and the difference extinction coefficient for formation of $PL_{sq}^{\bullet}$ from $PL_{red}^-$ (∼5800 $M^{-1}$ $cm^{-1}$) is around 7400 $M^{-1}$ $cm^{-1}$. This is less than half of the 16 000 $M^{-1}$ $cm^{-1}$ value responsible for the ground-state bleach after excitation (the excited-state absorption component of the signal will decay with a rate constant $k_{eT}$ upon electron transfer from $^1PL_{red}^-$ to the CPD). Therefore, a quantitative recovery of the bleach to a $\Delta A$ of 0 is not expected for electron transfer only. On the basis of these considerations, we assign the 32 ps lifetime as the electron-transfer lifetime [$\tau_1 = \tau_{eT} = (k_{eT})^{-1}$ (**2** → **3**, Scheme 1)], which is ∼3 times shorter than that previously measured for the thymidine dimer substrate (*7*).

Having accounted for the electron-transfer step, we suggest that the recovery of the transient up to and beyond a $\Delta A$ of 0 is indicative of the repair of the substrate. In the absence of repair, the signal should reach a level corresponding to a $\Delta\epsilon$ of approximately −5800 $M^{-1}$ $cm^{-1}$ because of the $FADH^- \rightarrow FADH^{\bullet}$ conversion. However, the zero crossing at ca. 60 ps suggests that one of the C═C bonds of the substrate is re-formed almost immediately after electron transfer (**3** → **4**, Scheme 1) and that the rate of this process is limited by the electron-transfer lifetime. This is true only if there are no other intermediates that have a comparable transient absorption strength. A possibility is that the zero crossing is due to electron transfer from the isoalloxazine to the adenine moiety, or to a nearby tryptophan molecule (e.g., Trp286 in *A. nidulans*). However, Trp radicals have very low extinction coefficients in this region of the spectrum (*36*). In addition, if electron transfer involves either an amino acid residue or the adenine, then this spectral signature should be seen upon excitation of the protein without substrate. This was not observed. Thus, we think that the zero crossing reflects the absorption of the repaired substrate following electron transfer. This suggests that one C═C bond is formed almost immediately upon electron transfer with little or no activation barrier.

Although the zero crossing for the decay of the pentameric substrate−protein complex occurs within ∼60 ps, the signal continues to increase until a maximum is reached around 1500 ps with a modest decay of absorption out to the 3000 ps limit of the scan. The same trend is also seen for the 20:1 molar ratio experiment using $d(T<>T)_2$ and comes out of the fitting of the decays for all experiments with substrate. We deal with this issue below. The increase to 1500 ps is much more than five electron-transfer lifetimes (∼160 ps). Furthermore, the magnitude of $\Delta A$ at 1500 ps is comparable to the magnitude of $\Delta A$ for the initial bleach. If repair is complete, then we expect the change in the extinction coefficient due to the C═C bonds ($\Delta\epsilon_{C=C}$) to be ∼2 × 9500 $M^{-1}$ $cm^{-1}$ (19 000 $M^{-1}$ $cm^{-1}$) at this wavelength. Thus, we expect that the absolute change in absorption due to repair at the probe wavelength will be slightly more than the ground-state bleach. It is seen that this is roughly the case. A proper analysis of the absorption change will have to take into account the relative orientation of the $FADH^-$ and $CPD^{\bullet-}$ transition dipole moments. In addition, it is likely that the maximum $\Delta A$ is due to the formation of $T-T^{\bullet-}$ as opposed to T−T (**4** → **5**, Scheme 1). However, within these constraints, the observed $\Delta A$ corroborates the assignment that the 265 nm transient is due primarily to repair of the CPD and does not represent spectroscopic changes due to the flavin or the protein. Taken together, these results imply that a second repair step is occurring with a lifetime much longer than 100 ps. A rough estimate would be 600 ps, the time constant obtained as the second component of the fit. These results are in contrast to those obtained by Kim *et al*. (*13*),

who observed a 420 nm transient with a lifetime of 0.5−2 ns for the U<>T but not for the T<>T substrate.

The slight decrease in absorption after 1500 ps is suggestive of electron transfer from $T-T^{\bullet-}$ to an unidentified acceptor. This interpretation is supported by the work of Yeh and Falvey (*3*), who showed that $T-T^{\bullet-}$ has a greater extinction coefficient than T−T at 265 nm. It has been assumed that electron transfer from the repaired substrate supplies the reducing equivalent for the flavin cofactor: $T-T^{\bullet-} + PL_{sq}^{\bullet} \rightarrow T-T + PL_{red}^{-}$ (**5** → **6**, Scheme 1). However, the observation of semiquinone buildup in our fast pulse experiments suggests that the final electron acceptor for the excess electron on $T-T^{\bullet-}$ is not the flavin cofactor, and that $FADH^{\bullet}$ is reduced by another mechanism. This is discussed below.

## DISCUSSION

In 1990, Jorns and co-workers observed a blue shift in the absorption spectrum of oxidized photolyase bound to a CPD in a $T_{18}$ oligo (*27*). We reproduced these experiments and constructed a model (*15*) that suggests that the spectral shift is electrochromic in origin and due to the interaction of the substrate dipolar electric field with the difference dipole moments of the FAD cofactor (*38*). Interestingly, the spectral shift was absent when a dinucleotide substrate was used, even at concentrations where the equilibrium association constant predicted that the protein should be fully loaded with substrate (*23*). In this work, a spectral shift was measured with the $d(T<>T)_5$ substrate which was similar to that obtained for the $T_{18}$ oligo. Work by Jorns *et al*. (*32*) and Kim and Sancar (*23*) reported a dependence of photolyase repair activity on substrate length and concentration. Corroboration of this is provided by the higher yield of repair for the pentameric substrate found in this work. Thus, it is clear from our results that this substrate length dependence must be taken into account to properly interpret the kinetics and mechanism of the repair reaction.

Earlier measurements of the electron-transfer lifetime were obtained by time-correlated single-photon counting (TCSPC) in the presence of low molar ratios of substrate to protein. *E. coli* photolyase, using either $d(T<>T)_2$ or $d(T<>T)_{15}$ substrates (*10*), gave an electron-transfer lifetime $\tau_{eT}$ of ∼140 ps. The TCSPC experiments had a resolution of 80 ps with an excitation pulse width of 30 ps. From our results, it is not clear why the lifetime obtained for the $d(T<>T)_{15}$ substrate was the same as that for the dinucleotide substrate. TCSPC experiments on *A. nidulans* photolyase and $d(T<>T)_2$ substrate at saturating concentrations (*12*) gave the same lifetime using 30 ps resolution. In both cases, a longer-lived component was assigned to free protein but the 7 ps component for $PL_{red}^{-}$ measured in this work was not observed.

The transient absorption experiments of Okamura *et al*. (*11*) were carried out with 12 ps resolution but used low dinucleotide substrate:protein molar ratios. We repeated these experiments with a $d(T<>T)_{18}$ substrate and obtained essentially the same result using a white light continuum probe with 300 fs resolution (data not shown). No HeNe laser was used in our experiment to avoid semiquinone buildup. In both experiments, photoreduction of the semiquinone would wash out any positive absorption changes around the 580 nm semiquinone absorption, eliminating evidence of a long-lived semiquinone after repair.

Langenbacher *et al*. (*7*) acknowledged the possibility of an uncomplexed enzyme in their 100 ps resolution transient absorption experiments using a visible wavelength probe. They fitted their data to two exponentials, assigning the fast component to substrate-bound photolyase and the slower component to unbound enzyme. These experiments used dinucleotide substrates with folate-reduced *E. coli* photolyase in a 5:1 molar ratio. The electron-transfer rate obtained for the T<>T lesion was $(100^{70}_{-50}\ \text{ps})^{-1}$, ∼3 times longer than that obtained in this study for the same substrate at a 20:1 molar ratio. Again, the 100 ps pulse width would be effective at photoreducing some of the semiquinone formed by excitation, leading to a mixture of populations undergoing ultrafast dynamics. They did report a ca. 50 ps component for the U<>U dimer, but it is not clear whether this component was due to repair or photoreactivation of $FADH^{\bullet}$ (see below).

The difference in behavior with regard to semiquinone buildup needs to be addressed as well. Langenbacher *et al*. found that reduced *E. coli* photolyase oxidized to the semiquinone ($PL_{red}^{-} \rightarrow PL_{sq}^{\bullet}$) at intensities above 100 $\mu J/mm^2$ regardless of whether substrate was present or absent. We also found that photooxidation occurred in *A. nidulans*, but only in the *presence* of substrate, even though the excitation intensity in our experiments was higher than that of Langenbacher *et al*. In our experiments, reduced *A. nidulans* photolyase was stable to oxidation in the absence of substrate and oxygen. There are other significant differences between the two experiments. Perhaps the most important difference lies in the structure of the antenna chromophore domain following the removal of this pigment. As was stated above, *A. nidulans* is overexpressed in *E. coli* without the antenna chromophore. Chemical reduction of the folate with borohydride (*39*) was used to remove this molecule from *E. coli* photolyase (*7*). However, this approach may compromise the structural integrity of the folate-binding domain of the protein (*39*). It is possible that this also leads to a compromised ability to retain the hydroquinone state under irradiation. It will be interesting to use *E. coli* protein that has been folate-depleted by gentler methods (*27*, *40*) to see if this is indeed the case. Still, this discrepancy is unresolved, and further experiments are needed to understand whether semiquinone buildup is an artifact of our experimental conditions or whether it signals a reassessment of the commonly accepted catalytic cycle as given for the **5** → **6** conversion in Scheme 1.

The use of longer pulses excitation might also hide the semiquinone buildup we observed in our experiments. The results of Aubert *et al*. have shown that the initial electron-transfer step in photoreactivation ($^2PL_{sq}^{\bullet} \rightarrow PL_{red}^{-}$) has a lifetime of ∼30 ps for *E. coli* PL (*14*). Taken together with our results, it appears that photoreduction of the flavin semiquinone will occur nearly simultaneously with repair for experiments that utilize laser pulses of greater than ∼30 ps. Since we measured no reactivation of $PL_{sq}^{\bullet}$ under our experimental conditions, it is possible that the longer time constants associated with electron transfer by tryptophan radicals during inadvertent photoreactivation could be averaged into data obtained with longer photolysis pulses and

exacerbated by repeated photolysis of the same sample volume.

It is premature, however, to conclude that back electron transfer from the repaired substrate to the flavin cofactor is not the pathway for reactivation of the flavin semiquinone for the next catalytic cycle. Our time-resolved experiments, with evidence of semiquinone buildup, are at odds with steady-state quantum yield experiments from several laboratories that give repair quantum yields between 0.7 and 0.9 (*41*−*43*). Such a high yield would be inconsistent with the requirement for a second photon to photoreduce the flavin semiquinone to its catalytically relevant state. On the other hand, theory (*44*, *45*) and experiment (*46*) suggest that thymidine radical anions are stabilized by adjacent bases *via* resonance. This stabilization may play an important role in the final repair step of the CPD after bond scission by photolyase. Although a thymidine radical anion is undesirable with regard to DNA integrity, the environment of the cell could easily provide an acceptor for the excess electron. In addition, reduction of the semiquinone from a different chemical source would be consistent with the measured repair quantum yields. Experiments designed to address these issues are planned.

The much faster electron-transfer lifetime found in this work, 32 ps, requires a rethinking of the electronic coupling between the $^1FADH^-$ and the initial acceptor. This in turn suggests that the initial acceptor may be much closer to the flavin than predicted by most theoretical treatments (*47*−*49*). As such, our results qualitatively support the experimental work of Park *et al*. (*50*), Berg and Sancar (*51*), and our group (*15*), as well as the theoretical treatment of Antony *et al*. (*52*). All of these studies are based on the *E. coli* protein so it is possible that the difference in electron-transfer kinetics between *A. nidulans* and *E. coli* photolyase accounts for the discrepancy, though we think that this is unlikely.

Our data do not as yet allow us to assign the identity of the initial acceptor, but the 60 ps zero crossing suggests that repair of the CPD begins by this time. If this is the case, it implies that the energy barrier for the first bond scission (C5−C5′ or C6−C6′) may be low or zero. However, given that $\Delta A$ increases up to 1500 ps, more than $5 \times 1/e$ times the zero crossing obtained in the pentameric kinetics, it does not seem likely that both C═C bonds are re-formed immediately after electron transfer. These data suggest that repair proceeds sequentially rather than in a concerted fashion and that the there is a significant barrier for the second step in the process. Interestingly, Langenbacher *et al.* have measured an activation barrier of 0.45 eV for bond splitting in *E. coli* PL for the U<>T dinucleotide substrate (*7*). Using a lifetime of 600 ps at room temperature this activation energy gives a prefactor of $\sim 9 \times 10^{16}$ $s^{-1}$. This is much higher than expected for any vibrational frequency that might become the coordinate for the transition state.

To gain further insight into the CPD repair mechanism will require higher signal-to-noise data using the approach employed herein. However, we expect that a visible light probe coupled with the use of the HeNe laser to keep the protein reduced will yield a representation of the repair intermediates that is more accurate than what has been possible. The use of a broadband probe under these conditions will allow for the measurement of decay-associated spectra that will give more information about the intermediates in the reaction. With the insights gained from this work, we hope that such experiments will lead to a convincing model of the repair mechanism in photolyase.

## CONCLUSION

Our results suggest that previous kinetic measurements using dinucleotide substrates may have been sensitive to only a fraction of enzyme−substrate complexes that exhibit the true electron-transfer and repair kinetics of this system. This interpretation is supported by the absence of a blue shift in the $d(T<>T)_2-PL_{ox}$ complex and by the dependence of the electron-transfer and repair kinetics on the concentration of small CPD substrates. Ultraviolet transient absorption kinetics show a fast (ca. 32 ps) exponential decay component that represents the rate of electron transfer from enzyme to substrate. The time scale for this event is much shorter than previously considered and suggests that the cofactor−substrate distance is shorter than previously thought. Our results also suggest that repair takes place by a sequential mechanism and that the first bond-breaking step is nearly activation-less. Finally, the evidence suggests that, at least for *A. nidulans* photolyase, the flavin cofactor might remain in the semiquinone state following repair. The $PL_{sq}^{\bullet} \rightarrow PL_{red}^{-}$ reactivation would then occur by a subsequent reduction event that is distinct from the repair process. Whether this step is photoactivated, either *in vivo* or *in vitro*, remains to be elucidated.

## ACKNOWLEDGMENT

We thank Professor Daniel Falvey and Professor Aziz Sancar for useful discussions. We also thank the reviewers for their helpful suggestions.

## REFERENCES

1. Sancar, A. (1994) *Biochemistry 33*, 2−9.
2. Hartman, R. F., Van Camp, J. R., and Rose, S. D. (1987) *J. Org. Chem. 52*, 2684−2689.
3. Yeh, S. R., and Falvey, D. E. (1991) *J. Am. Chem. Soc. 113*, 8557−8558.
4. Heelis, P. F., Okamura, T., and Sancar, A. (1990) *Biochemistry 29*, 5694−5698.
5. Jordan, S. P., and Jorns, M. S. (1988) *Biochemistry 27*, 8915−8923.
6. Heelis, P. F., Kim, S. T., Okamura, T., and Sancar, A. (1993) *J. Photochem. Photobiol., B 17*, 219−228.
7. Langenbacher, T., Zhao, X., Bieser, G., Heelis, P. F., Sancar, A., and Michel-Beyerle, M. E. (1997) *J. Am. Chem. Soc. 119*, 10532−10536.
8. Heelis, P. F., and Sancar, A. (1986) *Biochemistry 25*, 8163−8166.
9. Okamura, T., Sancar, A., Heelis, P. F., Hirata, Y., and Mataga, N. (1989) *J. Am. Chem. Soc. 111*, 5967−5969.
10. Kim, S. T., Heelis, P. F., Okamura, T., Hirata, Y., Mataga, N., and Sancar, A. (1991) *Biochemistry 30*, 11262−11270.
11. Okamura, T., Sancar, A., Heelis, P. F., Begley, T. P., Hirata, Y., and Mataga, N. (1991) *J. Am. Chem. Soc. 113*, 3143−3145.
12. Kim, S. T., Heelis, P. F., and Sancar, A. (1992) *Biochemistry 31*, 11244−11248.
13. Kim, S.-T., Volk, M., Rousseau, G., Heelis, P. F., Sancar, A., and Michel-Beyerle, M.-E. (1994) *J. Am. Chem. Soc. 116*, 3115−3116.
14. Aubert, C., Vos, M. H., Mathis, P., Eker, A. P. M., and Brettel, K. (2000) *Nature 405*, 586−590.
15. MacFarlane, A. W., IV, and Stanley, R. J. (2001) *Biochemistry 40*, 15203−15214.
16. Aubert, C., Mathis, P., Eker, A. P., and Brettel, K. (1999) *Proc. Natl. Acad. Sci. U.S.A. 96*, 5423−5427.

17. Aubert, C., Brettel, K., Mathis, P., Eker, A. P. M., and Boussac, A. (1999) *J. Am. Chem. Soc. 121*, 8659−8660.
18. Fisher, G. J., and Johns, H. E. (1976) in *Photochemistry and Photobiology of Nucleic Acids* (Wang, S. Y., Ed.) pp 226−294, Academic Press, New York.
19. Takao, M., Oikawa, A., Eker, A. P. M., and Yasui, A. (1989) *Photochem. Photobiol. 50*, 633−637.
20. Malhotra, K., Kim, S. T., Walsh, C., and Sancar, A. (1992) *J. Biol. Chem. 267*, 15406−15411.
21. Jorns, M. S., Wang, B., and Jordan, S. (1987) *Biochemistry 26*, 6810−6816.
22. Heelis, P. F., Payne, G., and Sancar, A. (1987) *Biochemistry 26*, 4634−4640.
23. Kim, S. T., and Sancar, A. (1991) *Biochemistry 30*, 8623−8630.
24. Wang, B., and Jorns, M. S. (1989) *Biochemistry 28*, 1148−1152.
25. Yasui, A., Takao, M., Oikawa, A., Kiener, A., Walsh, C. T., and Eker, A. P. M. (1988) *Nucleic Acids Res. 16*, 4447−4463.
26. Sancar, G. B., Smith, F. W., Lorence, M. C., Rupert, C. S., and Sancar, A. (1984) *J. Biol. Chem. 259*, 6033−6038.
27. Jorns, M. S., Wang, B., Jordan, S. P., and Chanderkar, L. P. (1990) *Biochemistry 29*, 552−561.
28. Ho, P. P., and Alfano, R. R. (1979) *Phys. Rev. A 20*, 2170−2187.
29. Anfinrud, P., Crackel, R. L., and Struve, W. S. (1984) *J. Phys. Chem. 88*, 5873−5882.
30. Du, M., Rosenthal, S. J., Xie, X., DiMagno, T. J., Schmidt, M., Hanson, D. K., Schiffer, M., Norris, J. R., and Fleming, G. R. (1992) *Proc. Natl. Acad. Sci. U.S.A. 89*, 8517−8521.
31. Stanley, R. J., King, B., and Boxer, S. G. (1996) *J. Phys. Chem. 100*, 12052−12059.
32. Jordan, S. P., Alderfer, J. L., Chanderka, L. P., and Jorns, M. S. (1989) *Biochemistry 28*, 8149−8153.
33. Heelis, P. F., Hartman, R. F., and Rose, S. D. (1993) *Photochem. Photobiol. 57*, 1053−1055.
34. Enescu, M., Lindqvist, L., and Soep, B. (1998) *Photochem. Photobiol. 68*, 150−156.
35. Stanley, R. J., and MacFarlane, A. W., IV (2000) *J. Phys. Chem. A 104*, 6899−6906.
36. Bent, D. V., and Hayon, E. (1975) *J. Am. Chem. Soc. 97*, 2612−2619.
37. Hayon, E. (1969) *J. Chem. Phys. 51*, 4881−4892.
38. Stanley, R. J., and Siddiqui, M. S. (2001) *J. Phys. Chem. A 105*, 11001−11008.
39. Jorns, M. S., Wang, B., and Jordan, S. (1987) *Biochemistry 26*, 6810−6816.
40. Payne, G., Wills, M., Walsh, C., and Sancar, A. (1990) *Biochemistry 29*, 5706−5711.
41. Sancar, G. B., Jorns, M. S., Payne, G., Fluke, D. J., Rupert, C. S., and Sancar, A. (1987) *J. Biol. Chem. 262*, 492−498.
42. Payne, G., and Sancar, A. (1990) *Biochemistry 29*, 7715−7727.
43. Ramsey, A. J., Alderfer, J. L., and Jorns, M. S. (1992) *Biochemistry 31*, 7134−7142.
44. Voityuk, A. A., Michel-Beyerle, M. E., and Rösch, N. (2001) *Chem. Phys. Lett. 342*, 231−238.
45. Al-Jihad, I., Smets, J., and Adamowicz, L. (2000) *J. Phys. Chem. A 104*, 2994−2998.
46. Hendricks, J. H., Lyapustina, S. A., de Clercq, H. L., and Bowen, K. H. (1998) *J. Chem. Phys. 108*, 8−11.
47. Hahn, J., Michel-Beyerle, M.-E., and Rösch, N. (1999) *J. Phys. Chem. B 103*, 2001−2007.
48. Sanders, D. B., and Wiest, O. (1999) *J. Am. Chem. Soc. 121*, 5127−5134.
49. Weber, S., Moebius, K., Richter, G., and Kay, C. W. M. (2001) *J. Am. Chem. Soc. 123*, 3790−3798.
50. Park, H.-W., Kim, S.-T., Sancar, A., and Deisenhofer, J. (1995) *Science 268*, 1866−1872.
51. Berg, B. J. V., and Sancar, G. B. (1998) *J. Biol. Chem. 273*, 20276−20284.
52. Antony, J., Medvedev, D. M., and Stuchebrukhov, A. A. (2000) *J. Am. Chem. Soc. 122*, 1057−1065.

BI034015W